SYNTHETIC BIOLOGY

Autonomous synthesis and assembly of a ribosomal subunit on a chip

Michael Levy, Reuven Falkovich, Shirley S. Daube*, Roy H. Bar-Ziv*

Ribosome biogenesis is an efficient and complex assembly process that has not been reconstructed outside a living cell so far, yet is the most critical step for establishing a self-replicating artificial cell. We recreated the biogenesis of *Escherichia coli's* small ribosomal subunit by synthesizing and capturing all its ribosomal proteins and RNA on a chip. Surface confinement provided favorable conditions for autonomous stepwise assembly of new subunits, spatially segregated from original intact ribosomes. Our real-time fluorescence measurements revealed hierarchal assembly, cooperative interactions, unstable intermediates, and specific binding to large ribosomal subunits. Using only synthetic genes, our methodology is a crucial step toward creation of a self-replicating artificial cell and a general strategy for the mechanistic investigation of diverse multicomponent macromolecular machines.

INTRODUCTION

Ribosomes are the universal decoders of the genetic code that synthesize all cellular proteins in all life forms. Ribosomes are unique biological machines composed of dozens of proteins and RNAs, which synthesize their own parts and assemble in a sophisticated stepwise process. Ribosome assembly has been studied for decades to elucidate the composition of intermediates, assembly order, thermodynamics, and kinetics of assembly (*1*–*5*), yet there is no reconstituted system of ribosomes synthesizing ribosomes to date. Establishing a scenario for the autonomous assembly of nascent ribosomal proteins (r-proteins) and ribosomal RNA (r-RNA) into intact ribosomes coupled to their synthesis is the most crucial step for realizing de novo synthesis of functional ribosomes, which would lead to the bottom-up creation of a minimal self-replicating model of a cell (*6*–*8*).

Previously, nonautonomous ribosome assembly has been demonstrated with purified r-proteins coupled to synthesis of only the r-RNA (*9*–*11*). In the absence of ribosomes, correct assembly of the ribosomal subunits could be demonstrated in these studies by measuring the capacity of nascent subunits to catalyze peptide bond formation. Recently, the dynamics of assembly of subdomains of the small ribosomal subunit (SSU) have been measured by monitoring binding of purified r-proteins to nascent r-RNA molecules, cotranscriptionally, at single-molecule resolution (*12*, *13*).

We sought an experimental scheme that would allow expression of all parts of the *Escherichia coli* SSU at sufficiently high concentrations to drive interactions, which amounts to 20 r-proteins (S2-S21), one r-RNA (16*S*), and six assembly factors (Era, RsgA, RbfA, RimM, RimN, and RimP), which have been shown to promote in vitro SSU assembly (*10*), thus challenging the capacity of a cell-free minimal protein synthesis system (*14*). Previously, we have shown that genes immobilized on the surface of a chip in the form of DNA brushes localize the transcription-translation machineries (RNA polymerases and ribosomes, respectively), becoming a local source for nascent RNA and proteins despite the minute amount of DNA in the bulk reaction (*15*, *16*). We thus reasoned that r-proteins, r-RNA, and assembly factors synthesized from DNA brushes would localize at sufficiently high concentrations to drive ribosomal subunit assembly (Fig. 1A and figs. S1 and S2).

To deduce on-chip assembly, we relied on years of elaborate biochemical and biophysical analysis, revealing a process of 20 r-proteins binding onto a single long r-RNA, shaping its folding pathway all the way into the mature SSU (*17*). This orchestrated pathway displays two signatures. One is the classification of r-proteins according to their binding dependence on the presence of other r-proteins, with the binding of secondary and tertiary r-proteins contingent on the prebinding of primary and secondary binders (Fig. 1B) (*1*, *2*); the other is the kinetic order by which r-proteins join the complex (*18*). We identified these signatures in our cell-free reaction, allowing us to confirm autonomous on-chip assembly of the *E. coli* SSU and to reveal new insights into the assembly mechanism.

RESULTS

Ribosomal parts synthesized from surface-immobilized gene brushes

We first tested the capacity of each r-protein to be expressed and bind the r-RNA from surface-immobilized genes. The r-RNA was modified with a Broccoli aptamer sequence inserted in helix 6 (H6) (*19*) for its in situ labeling and imaging (*20*) by total internal reflection fluorescence (TIRF) microscopy and a ribozyme sequence at the 3′ end for synthetic processing by self-cleavage (Materials and Methods and fig. S3, A to C) (*21*). All r-proteins were tagged with a hemagglutinin (HA) peptide (r-protein–HA), targeting them to surface-immobilized anti-HA antibodies for further localization and sensitive detection (Materials and Methods, fig. S3D, and table S1). Genes of each r-protein–HA were mixed with the r-RNA genes and immobilized as a three-brush cluster, resulting in 20 different clusters on the same surface (Fig. 1C and movie S1). We added a minimal gene expression reaction mix made from purified components (*22*) and heated the chamber to 37°C. An r-RNA fluorescence signal appeared, propagating radially from the three central brushes and accumulating on surface antibodies in a hexagonal pattern that helped identifying specific signals with high sensitivity (Fig. 1C, figs. S1 and S2, and movie S2). The signal was enhanced by the addition of a molecular crowding reagent found to enhance multicomponent interactions (*23*) and was sensitive to the r-protein–HA:r-RNA genes ratio within the central brushes, reducing to background levels in the absence of r-protein–HA genes

Department of Chemical and Biological Physics Weizmann Institute of Science, Rehovot 7610001, Israel.
*Corresponding author. Email: shirley.daube@weizmann.ac.il (S.S.D.); roy.bar-ziv@weizmann.ac.il (R.H.B.-Z.)

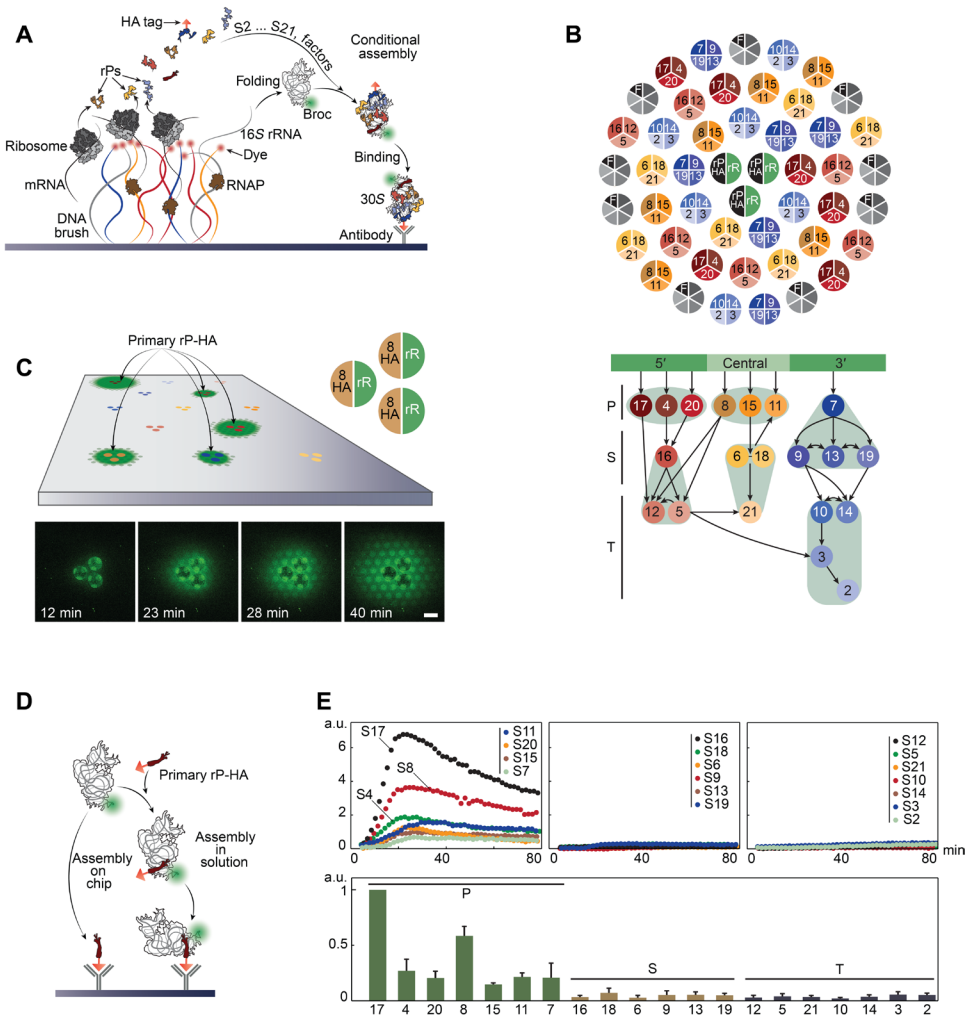

Fig. 1. A genetic program for ribosome assembly on a chip. (**A**) Scheme: r-RNA (in situ fluorescently labeled; green spot), r-proteins, and assembly factors expressed from gene brushes assemble and bind to surface anti-HA antibodies through an HA tag on one of the r-proteins (orange triangle). (**B**) A radial brush layout (top scheme) of r-RNA (green) and r-protein–HA (black) genes in the central three-brush cluster, surrounded by gene brushes of six assembly factors (grayscale) and all other r-proteins (RGB-scale), related by color to the *E. coli* assembly map [bottom scheme; based on (*4*) and (*18*)]. r-proteins in the same brush are shaded green, classified as primary, secondary, or tertiary, and as 5′, central or 3′ domains of the r-RNA (green line). Arrows indicate the dependency order. (**C**) Top: Twenty three-brush clusters on the same surface, each with a different r-protein–HA gene, produce variable r-RNA signals. Bottom: Fluorescent images of r-RNA binding to S8-HA at four time points. Scale bar, 100 μm. (**D**) r-RNA can bind to r-protein–HA on the surface or in solution before surface binding. (**E**) Signal dynamics of r-RNA interaction with primary (P) (left), secondary (S) (center), and tertiary (T) (right) r-protein–HAs in the absence of assembly factors. Bottom: f_{max} of each primary, secondary, and tertiary r-protein–HAs. Error bars are standard deviation (SD) of three repeats. Time intervals are averages of three repeats. a.u., arbitrary units.

(fig. S4), suggesting that binding of fluorescent r-RNA to surface antibodies was mediated by the r-protein–HA. For each r-protein–HA:r-RNA cluster, we plotted the time-dependent signal of emerging hexagonal patterns and recorded the maximal intensity (f_{max}) (Fig. 1E). In complete agreement with the assembly map (Fig. 1, B and D), the highest f_{max} was obtained for the primary r-protein–HAs, and very low yet measurable signals were obtained for the secondary and tertiary r-proteins (Fig. 1E, fig. S4D, and movie S3).

Timeline of ribosomal subunit assembly on a chip

To observe the assembly process of the entire SSU and substantiate the expression and functionality of the secondary and tertiary r-proteins, we arranged the genes coding for all r-proteins (with no HA tag) and six assembly factors in groups according to the assembly map and immobilized them as brushes surrounding the central three-brush cluster, with genes of the central r-protein–HA omitted from surrounding brushes (Figs. 1B and 2A). Anticipating low signals due to expression and interactions of 27 different molecules, we reduced the thickness of the chamber to further confine the reaction (table S2).

We recorded the f_{max} values for each layout and found that the primary r-proteins again displayed the highest values, with signals of secondary and tertiary r-proteins much enhanced compared with the minimal two-body analysis (Fig. 2, B and C, and movies S4 and S5), implying that binding of r-RNA to secondary and tertiary r-protein–HAs was mediated by other r-proteins. In addition, we recorded the onset time (t_0) of initial detection (fig. S1F) and aligned them from fast to slow, producing a kinetic timeline for SSU cell-free synthesis and assembly (Fig. 2D). We identified four kinetic binding groups,

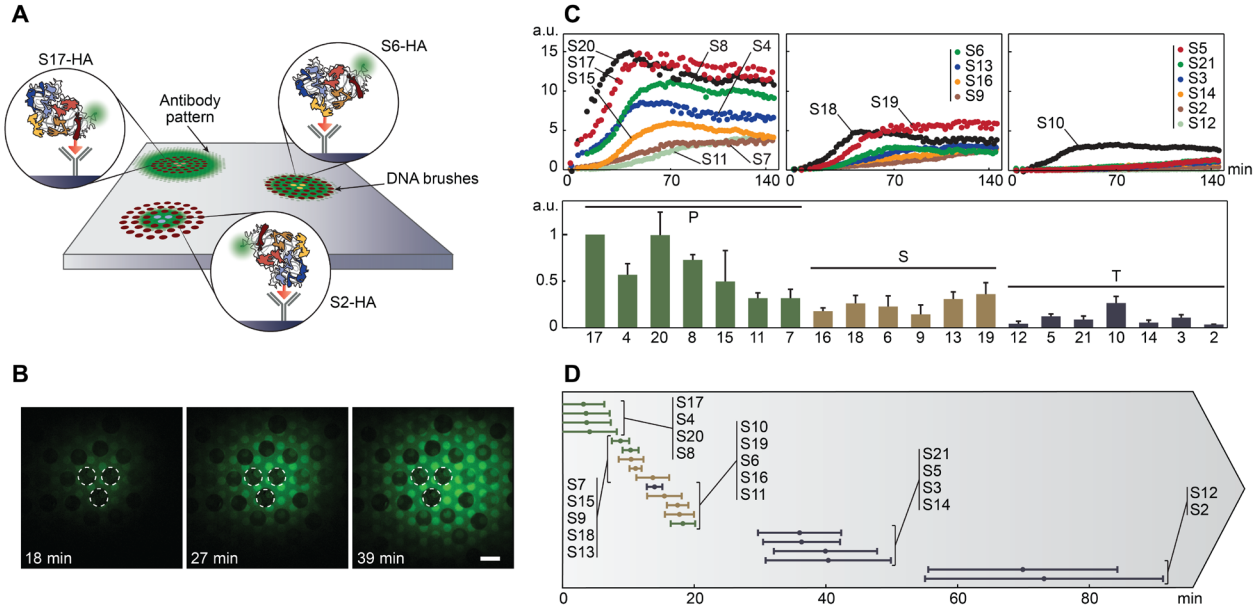

Fig. 2. *E. coli* SSU biogenesis on a chip. (**A**) Scheme: Twenty brush clusters coding for all SSU r-proteins, and the assembly factors Era, RsgA, RbfA, RimM, RimN, and RimP surround the central r-RNA and r-protein-HA brushes. (**B**) r-RNA fluorescent signal buildup in time for the S15-HA configuration. Scale bar, 100 μm. (**C**) Top: Signal dynamics of r-RNA binding to primary (left), secondary (center), and tertiary (right) r-proteins–HAs. Bottom: f_{max} of all r-proteins–HAs. (**D**) SSU t_0 timeline indicating the onset time of each r-RNA:r-protein–HA interaction. Error bars are SD of three repeats. Time intervals are averages of three repeats.

with t_0's highly overlapping within a group, consistent with previously observed multiple assembly pathways (*4*, *18*, *24*). For the most part, the t_0's timeline was comparable to in vitro assembly rates measured with purified r-proteins (*4*, *18*), with minor deviations, such as a slower binding of S16 than the rest of the 5′ domain primary r-proteins.

We verified that surface confinement was an essential prerequisite for successful assembly by repeating the experiment with only r-RNA genes immobilized on the surface, while r-protein genes were added to the cell-free reaction bathing the surface (fig. S5A). Despite the addition of high DNA concentrations to the cell-free reaction, on the order of 40 nM, appreciable signals of r-RNA around its brushes were detected only when primary r-proteins (S17-HA), but not tertiary genes (S2-HA), were used. Mixing S17-HA genes with genes coding for a non–r-protein decreased the r-RNA signal, most likely due to reduced expression levels of S17-HA by competition over the gene expression machinery. On the other hand, synthesis of ribosomal parts from brush layouts that were at an effective volumetric concentration of 70 pM could reach sufficiently high local concentrations without saturating the transcription-translation machinery, suggesting that even more genes could potentially be added in an on-chip reaction. In addition, we tested the effect of brush arrangements within a layout on r-RNA binding to S10-HA (fig. S5B), always keeping the number of brushes constant. A drop in the signal was observed when the radius of layout was increased but was not affected by reshuffling brushes, suggesting that assembly yield was determined by the local concentration of r-proteins and r-RNA above each layout, dictated by the DNA density on the surface.

Assembly hierarchy by on-chip deletions of gene brushes

To gain evidence that r-RNA signal obtained on immobilized secondary r-proteins was mediated by other r-proteins, we performed gene deletion experiments and revealed conditional binding patterns that comprise the assembly map (Fig. 3, A and B). We did so in the absence of assembly factors and in a bulk reaction chamber twice as thick (table S2), similar to the two-body experiment (Fig. 1, C to E), to reduce overall concentrations, allowing us to observe r-RNA:r-protein–HA interactions that are exclusively contingent on the presence of r-proteins. Although the use of fluorescently labeled r-proteins could directly demonstrate their participation in the assembly reaction (fig. S6), we continued to use the r-RNA as the sole fluorescently labeled species to quantitatively compare between different brush layouts. We scanned all possible primary and secondary r-protein combinations within the 5′, central, and 3′ domains for mediating r-RNA binding above the basal level of the two-body interactions (Fig. 3, C to E, and figs. S7 and S8). Each of these domains has been previously shown to assemble in vitro in the absence of others (*25*–*27*). In general, the data presented in Fig. 3 demonstrated that the 5′ and 3′ domains, including only the primary and secondary r-proteins, were formed stably onto the corresponding secondary r-proteins–HA as surface anchors (S16-HA, S9-HA, S13-HA, and S19-HA), while the signal corresponding to central domain assembly (onto S6-HA) was unstable and decreased after an initial accumulation.

Comparison of t_o and f_{max} values within each domain revealed binding dependencies, which, for the most part, adequately matched those previously documented, with some new features uncovered. Our analysis revealed a dependence of r-RNA binding to S6-HA on the presence of S18, which have been shown to form a dimer (Fig. 3C) (*28*). Binding of r-RNA to S6-HA was dependent cooperatively on the presence of both S15 and S18 and further enhanced by the addition of S8 (*1*, *29*). We further found that addition of S4, or to a lesser extent S20, facilitated r-RNA binding to S16-HA, and their combinations increased the signal additively (Fig. 3D) (*30*). Last, we found that in addition to previously characterized 3′ partial intermediates (*31*), the presence of the 3′ secondary r-proteins could facilitate strong binding to r-RNA in the absence of the primary r-protein S7 (Fig. 3E).

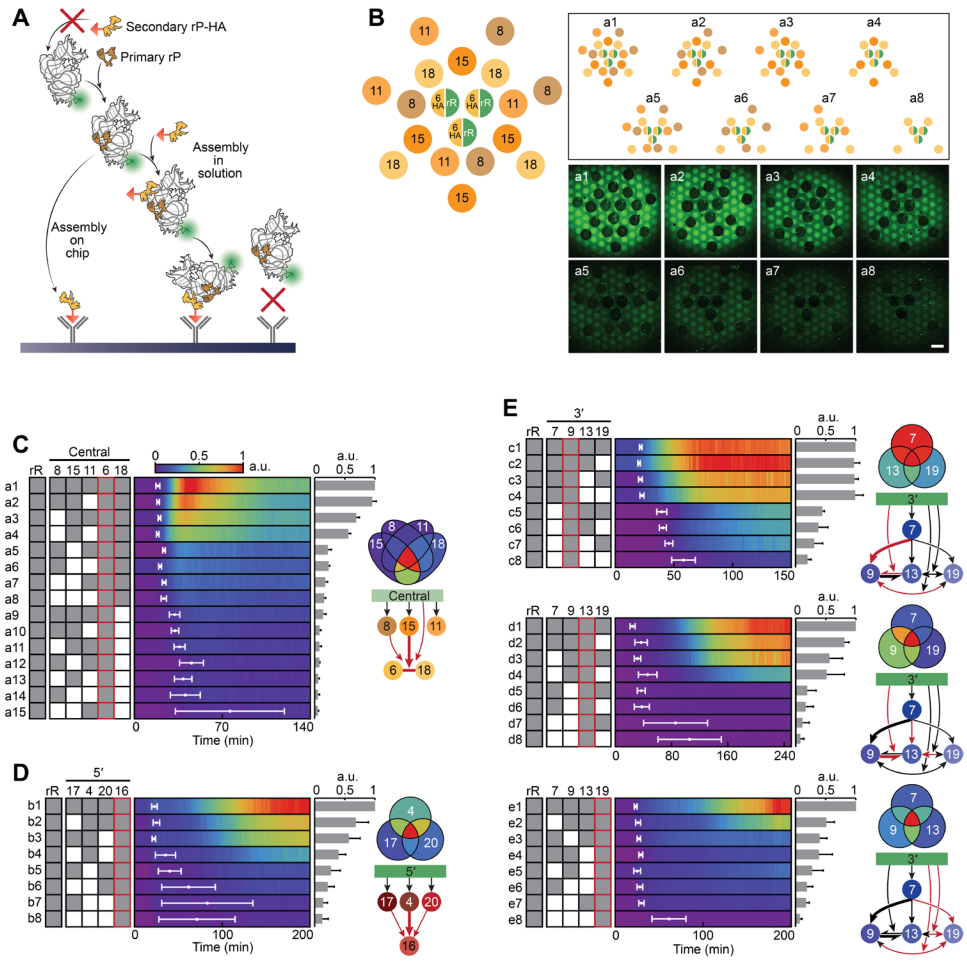

Fig. 3. Binding dependencies of *E. coli* secondary r-proteins. (**A**) Scheme: Two modes of r-RNA binding to r-protein–HA on the surface, dependent on prebinding of other r-proteins to the r-RNA, in the absence of assembly factors. (**B**) Brush layouts (a1 to a8) of central domain analysis (S6-HA) and the corresponding fluorescent images at $t = 45$ min. Scale bar, 100 μm. (**C** to **E**) Signal dynamics color maps of brush combinations, central (a1 to a15), 5′ (b1 to b8), and 3′ (c1 to c8, d1 to d8, e1 to e8) domains. White time intervals represent t_0. Gene combinations are depicted as gray and white boxes, indicating the presence or absence of an r-protein gene, respectively. Red frame indicates the r-protein–HA. Averaged f_{max} values are presented as bars at the end of each color map and as a Venn diagram according to the color scale. Error bars are SD of three repeats. Partial assembly maps depict in red the dependencies deduced from the corresponding study. Large arrows represent strong dependencies.

Late stages of small subunit assembly: Stability and binding to large subunit

S2-HA was one of the two slowest binders in our on-chip reaction (Fig. 2D), signifying late stages of SSU assembly, and we therefore analyzed its binding dependencies by deletions of groups of r-proteins and assembly factors (Fig. 4, A to C, and fig. S9). In the presence of the six assembly factors ("6F"), the strongest signal was obtained with all r-proteins present, but a fairly strong signal was also obtained with only the 5′ or 3′, but not the central, r-proteins (Fig. 4A). The assembly of S2-HA with r-proteins of the 3′ domain is consistent with previous observations (*27*) but, to our knowledge, has not been documented with the 5′ r-proteins.

To gain further insight into the role of assembly factors, we separated the factors into two groups, guanosine triphosphatases (GTPases) ("2F"; Era and RsgA) and non-GTPases ("4F"; RbfA, RimM, RimN, and RimP), and observed that even in the absence of r-proteins, some signal could be detected, but inclusion of r-proteins always enhanced it (Fig. 4B and movie S6). A much higher signal was obtained with the 2F compared with the 6F combination, suggesting that one or all of the 4F group exhibited an inhibitory effect on the r-RNA:S2-HA interaction, reminiscent of a recent observation that overexpression of RbfA (part of 4F) inhibited assembly in the absence of RsgA (part of 2F) (*32*). In addition, the signal obtained with both 2F and r-proteins was higher than the sum of signals with either one, suggesting that their mutual effect was cooperative.

We further found that an r-RNA:S2-HA signal, stable in time, was observed only in the presence of all r-proteins (Fig. 4C). In all deletion combinations, even in the absence of any r-proteins, a signal appeared but decreased with time, clearly demonstrating that participation of r-proteins from all domains was essential to obtain a stable SSU assembly (Fig. 4C, fig. S9, C and D, and movie S7). This experiment was performed in the absence of the two GTPases, which might have enhanced assembly, possibly masking the contribution of r-proteins. The unstable binding mode of r-RNA:S2-HA may represent an unstable intermediate, reminiscent of an interesting in vivo observation of early S2 binding to nascent r-RNA cotranscriptionally (*33*).

Last, we looked for the ability of de novo synthesized SSU to interact specifically with the large ribosomal subunit (LSU), as a hallmark

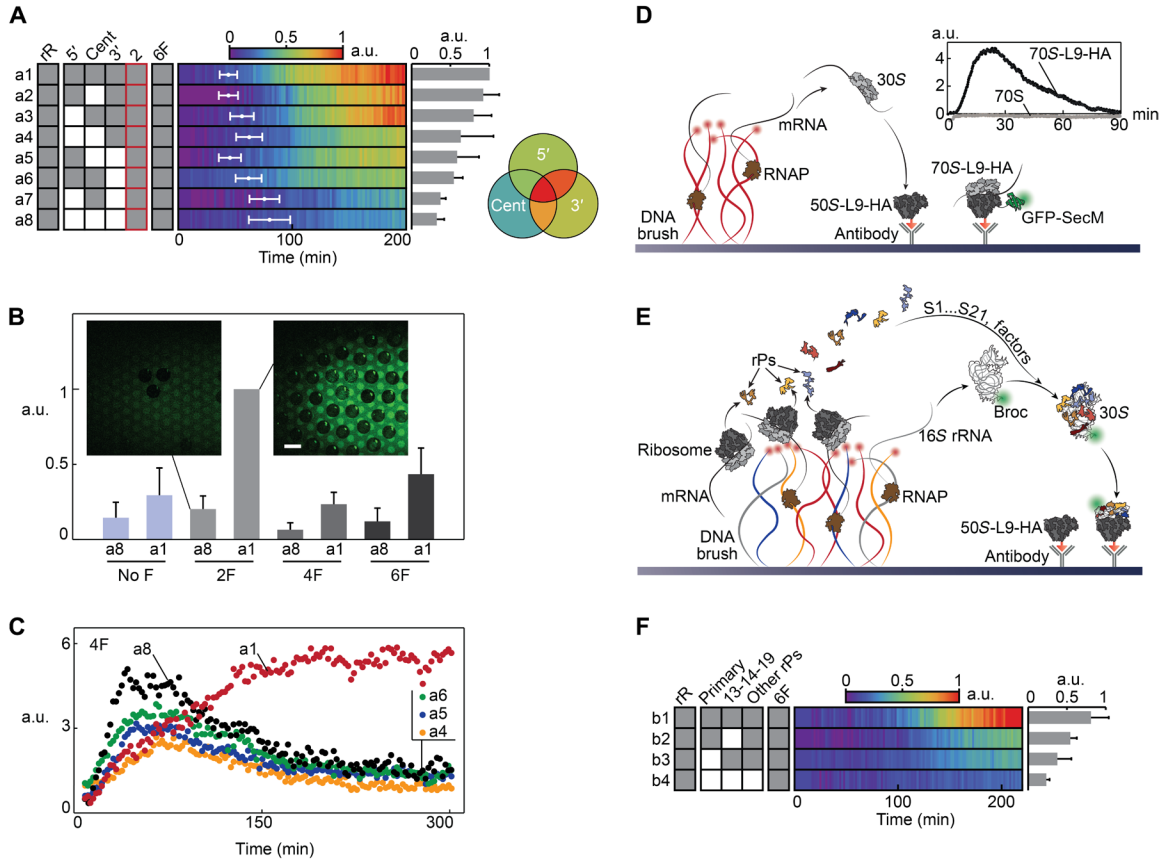

Fig. 4. Late stages of on-chip *E. coli* SSU assembly. (**A**) r-RNA:S2-HA signals for different combinations of SSU domains (a1 to a8), depicted as dynamic color maps. Labels are as in Fig. 3. (**B**) Averaged f_{max} values of r-RNA:S2-HA signals for different assembly factor combinations with and without all r-proteins. Error bars represent SD of three repeats. Scale bar, 100 μm. (**C**) Signal dynamics of r-RNA:S2-HA interactions in the presence of four factors and domain combinations. (**D**) Scheme: Ribosomes localized on surface antibodies actively engaged in GFP-SecM synthesis with purified SSU added from bulk solution. mRNA is produced from nearby DNA brushes. Inset: TIRF dynamic signal of GFP-secM on surface-bound ribosomes. (**E**) Scheme: Synthesis and assembly of nascent SSU and binding to surface immobilized LSUs. (**F**) Signal dynamics color maps of nascent SSU binding onto surface-bound LSU, dependent on different r-protein combinations (b1 to b4). In each panel, the presence of assembly factors is marked as 2F (Era and RsgA), 4F (RbfA, RimM, RimN, and RimP), or 6F (all).

for correct SSU assembly (*3*). To that end, purified ribosomes (*34*) modified with an HA tag on LSU's r-protein L9 (L9-HA) were bound to surface antibodies in patterned hexagons (Materials and Methods and fig. S10). In a preliminary experiment, these surface ribosomes were shown to be active by synthesizing green fluorescent protein (GFP) with a pause sequence (GFP-SecM) when supplemented by a purified SSU in solution (Fig. 4D, inset, and fig. S10) (*35*). A DNA brush layout including genes of r-RNA, all r-protein genes including S1, and all six assembly factors but no r-protein–HA resulted in a clear r-RNA signal on the immobilized ribosome pattern (Fig. 4, E and F, and fig. S10). A twofold decrease in signal was observed when either primary r-proteins or the intersubunit bridge-forming r-proteins (*36*) were deleted, suggesting that an intersubunit bridge was formed between the nascent SSU and the immobilized LSU.

DISCUSSION

Together, our data led us to conclude that the *E. coli* SSU was assembled on the chip and that the cell-free synthesis and assembly process took about 70 min (Figs. 2D and 4A), comparable to in vivo SSU reassembly from disassembled r-proteins after a thermal shock (*37*) or to previous in vitro SSU assembly systems using purified r-proteins (*4*). We speculate that miniaturization of the reaction chamber dimensions may increase the overall assembly rate by further increasing the local concentration of reaction components.

The ability to monitor the dynamics of stepwise ribosome assembly opens possibilities to look for enzymatic activities, such as protein and RNA modification enzymes, which may affect the rate and efficiency of the process, by simply incorporating their genes in the DNA brushes. The genotype/phenotype linkage of brush layouts allows to screen for mutations in r-proteins and r-RNA and other genetically encoded activities or small-molecule drugs that could modulate ribosome assembly. Comparative dynamics of SSU assembly from different organisms are feasible, as well as attempting to assemble hybrid ribosomes. The assembly process of other multicomponent complexes such as proteasomes, replisomes, divisomes, and viruses could be studied, although none is as challenging as the ribosome, a machine that synthesizes its own parts.

Symmetry breaking, inherent to our setup, with newly assembled SSUs anchored to the surface spatially resolved from original ribosomes, may prove an advantage in attempting to assess the full functionality of de novo assembled subunits. Our approach should be able to

support the synthesis of ribosomal parts of both the SSU and LSU, leading to the autonomous assembly of a full ribosome, a cornerstone for protein-based self-replicating artificial cells.

MATERIALS AND METHODS

DNA preparation

Cloning of E. coli r-RNA and r-protein genes in cell-free expression plasmids

Genes of *E. coli* 16*S* r-RNA and 30*S* r-proteins were amplified from the genome of *E. coli* K12 JM109 using KAPA HiFi HotStart ReadyMix (KAPA BIOSYSTEMS) and the appropriate primers [Integrated DNA Technologies (IDT); table S1]. Each primer was composed of a variable sequence specific to the cloned gene and a constant sequence of the target plasmid. Enzyme-free cloning was performed using Gibson Assembly Cloning Kit [New England Biolabs (NEB)] by replacing the DHFR (dihydrofolate reductase) gene under the T7 promoter in the PURExfrex2.0 system control vector (Cosmo Bio, Japan). For HA-tagged r-proteins, cloning was into pIVEX 2.5 (Roche) in frame with the C-terminal HA tag using primers with a constant sequence for insertion into the host plasmid and a variable sequence specific for each gene (table S1). For r-protein fluorescent in situ labeling (r-protein–UAG), the TAG codon was introduced into the pIVEX clones using forward primers with a similar variable sequence as in table S1 but with the TAG codon inserted between the ATG codon and the second codon of each gene. The r-RNA gene, without its leader sequence, was cloned into the PURE control vector immediately after the promoter sequence using appropriate primers (table S1).

Broccoli aptamer and HDV ribozyme genetic insertions into the 16S r-RNA gene

The Broccoli aptamer sequence (*20*) was inserted into H6 of the r-RNA, which has been shown to tolerate sequence insertions while maintaining ribosome function (*19*). Hepatitis delta virus (HDV) ribozyme sequence was inserted at the 3′ end of the 16*S* r-RNA to ensure formation of an exact 3′ end (*21*). For both Broccoli and HDV insertions, the PURE plasmid containing the r-RNA gene was amplified by inverse polymerase chain reaction (PCR) using phosphorylated forward (F) and reverse (R) primers (table S1), followed by ligation and transformation into competent *E. coli* DH5α.

In vitro synthesis of r-RNA and r-proteins in test-tube reactions

Plasmids coding for r-proteins–UAG with or without the HA tag were added to a 5-μl cell-free in vitro transcription translation reaction (PURExfrex2.0, Cosmo Bio, Japan) at 3 nM final concentration. The in vitro reactions were supplemented with transfer RNA with an amber codon charged with an unnatural fluorescent amino acid [CloverDirect 5-CR110-X amber (498), Cosmo Bio, Japan] according to the manufacturer's instructions. Reactions were incubated for 2 hours at 37°C and quenched by a fourfold dilution with sodium dodecyl sulfate (SDS) loading buffer [at a final concentration of 2% SDS, 10% glycerol, 5% 2-mercaptoethanol, 0.002% bromophenol blue, and 62.5 mM tris HCl (pH 6.8)]. A volume of 3 μl of each reaction was loaded on an 18% bis:acrylamide gel and resolved with 25 mM tris–192 mM glycine–2% SDS running buffer (fig. S3). Gels were scanned using an FLA-5100 scanner (FUJIFILM).

Linear PCR fragments coding for r-RNA with or without aptamer and ribozyme sequences, under T7 promoter but with no terminator sequence, were incubated at a final concentration of 3 nM in transcription buffer [80 mM tris-HCl (pH 7.8), 1 mM spermidine 2 mM dithiothreitol, and 15 mM $MgCl_2$]. The reaction was supplemented with rATP, rCTP, rGTP, and rUTP each at 5 mM, and T7 RNA polymerase (5 U/μl) (NEB). Transcription reactions with r-RNA–HDV or r-RNA–Broccoli were supplemented with Aminoallyl-UTP–ATTO-488 or Aminoallyl-UTP–ATTO-647N, respectively (Jena Bioscience) to a final concentration of 16.6 μM. After 1-hour incubation at 37°C, reactions were quenched with SDS loading buffer, and 5 μl was loaded on a 4-20% polyacrylamide gel (GeBa). Gels were run in 25 mM tris–192 mM glycine buffer and scanned using an FLA-5100 scanner (FUJIFILM) (fig. S3). For in-gel visualization, before scanning, the gel was washed three times for 5 min with water and then stained for 10 to 30 min in 10 μM DFHBI-1T (Lucerna) in 40 mM Hepes (pH 7.4), 100 mM KCl, and 1 mM $MgCl_2$ (*20*).

Preparation of linear DNA fragments for DNA brushes

Linear double-stranded DNA fragments were synthesized and conjugated to streptavidin (SA; S0677, Sigma-Aldrich) essentially as described in (*38*) and references therein. Briefly, a 5′–Alexa Fluor 647 forward primer (IDT) positioned ~200 base pairs (bp) upstream to the T7 promoter and 5′-biotin reverse-primer (IDT) positioned downstream to the T7 terminator were used to amplify genes by PCR with KAPA HiFi HotStart ReadyMix (KAPA BIOSYSTEMS). The distance of the 5′-biotin primer from the T7 terminator was variable, depending on gene length, to obtain similar overall length of ~1700 bp for all DNA fragments, except for r-RNA, which was 2400 bp long. Noncoding DNA was prepared similarly to coding DNA but without the T7 promoter. Biotinylated DNA was conjugated to SA at a 1:1.4 ratio at a final concentration of 150 nM in phosphate-buffered saline (1× PBS), supplemented with 7% glycerol to reduce evaporation at the following DNA surface deposition. Linear DNA fragments coding for GFP-uv3 under a T7 promoter, with a SecM arrest sequence, were amplified from the plasmid pETC1 (a gift of J. Puglisi) (*35*).

Ribosome preparation

The r-protein L9 of the LSU was amplified, similarly to SSU r-genes, and cloned into plasmid pRSFduet under control of T7 promoter/lac operator using the appropriate primers (IDT, table S1). An HA peptide sequence was cloned at its C terminus. L9-HA was overexpressed in BL21(DE3) grown in LB by induction with 1 mM isopropyl-β-D-thiogalactopyranoside (IPTG) at OD_{600} (optical density at 600 nm) of 0.25 to 0.35 for 3 hours. Cell lysis and ribosome purification were performed similarly to the method described in (*34*). Frozen cells were resuspended in ribosome buffer (RB) [10 mM tris-HCl, 70 mM KCl, and 10 mM $MgCl_2$ (pH ~7.8)], disrupted by short sonication on ice (Sonics VCX 750 Vibra Cell, tapered microtip, 40% amplitude, 5- to 15-s pulses, 60-s total sonication), and further lysed by passing through a French Press at 15kPSI at 4°C. The lysate was filtered and loaded on a quaternary amine monolith column (CIMmultusTM QA-8 ml, BIA Separations). After washing with RB + 0.35 M NH_4Cl, ribosomes were eluted by a gradient of 0.35 to 0.45 M NH_4Cl in RB. Ribosome fractions were collected and concentrated on a Vivaspin 20 10-kDa MWCO (molecular weight cutoff) concentration membrane (Sartorius), with buffer exchange to RB. Batches were brought to a final concentration of 20 to 25 μM, measured by ultraviolet (UV) absorption at 260 nm with an extinction coefficient of $4.2 \times 10^7\ M^{-1}$, in RB + 30% glycerol, frozen in liquid N_2, and stored at −80°C.

Biochip preparation

Photosensitive biocompatible monolayer coating

The protocol to form a photosensitive and biocompatible monolayer coating on fused-silica slides was described elsewhere (*38*). Briefly,

fused-silica slides (24 x 24 x 1 mm, UQG Optics) were cleaned in boiling ethanol (10 min) followed by sonication (10 min) and base piranha cleaning (H_2O_2:NH_3:H_2O, 1:1:4, heated to 70°C for 10 min). The slides were then coated with a polymer composed of a polyethylene glycol (PEG) backbone with a protected amine at one end and a triethoxysilyl group at the other end. The slides were incubated with a toluene solution of the polymer (0.2 mg/ml) for 20 min, rinsed with toluene, and dried.

UV patterning

The coated slides were exposed to 365-nm UV light (2.5 J/cm^2) through a custom photomask with an array of 40-μm hexagons (CAD/Art Services) using UV-KUB (Kloe) (fig. S2). The saturating UV dose fully deprotected surface amines inside hexagons. Surface amines located between hexagons were 53% deprotected due to leakiness of the mask (fig. S2). Biotin *N*-hydroxysuccinimidyl ester (EZ-link NHS-Biotin, Thermo Scientific) dissolved in borate buffer to a final concentration of 0.5 mg/ml was applied to the surface for 40 min and reacted with exposed amines. The slides were then washed with water and dried.

Biochip prism mounting and chamber preparation

The slides were fixed on custom fused silica prisms (Zell Quarzglas und Technische Keramik) with adhesive cutout of Frame-Seal Slide Chambers (Bio-Rad). The slit between prism and slide was filled with index-matching liquid (Cargille) before experiments. Rectangular chambers were cut in thin polydimethylsiloxane (PDMS) sheets (100 ± 30 μm) or in adhesive tape (50 ± 5 μm), depending on the desired height. The surface area of the chamber was of the order of 1 cm^2, depending on the specifics of each experiment.

DNA brush layout and deposition

Equimolar solutions of SA-conjugated linear DNA constructs were mixed at equal amounts according to the gene content, e.g., a mixed DNA solution of genes coding for S17, S4, and S20 had 33% of each. The exception was the central brushes with a mix of r-protein–HA and r-RNA genes. An optimal ratio to obtain the highest r-RNA signal was found empirically to be 10:1 r-RNA:r-protein–HA (fig. S4). Nanoliter droplets of these mixes were deposited in an automated way onto the biotin-patterned surface within the PDMS chamber using GIX Microplotter II (SonoPlot Inc., Middleton, WI) and 60-μm-diameter micropipettes (fig. S2C and movie S1). Every DNA mixture was deposited between five to seven times in each brush configuration to increase the concentration of expressed r-proteins. Droplets were incubated overnight in a humidity-controlled chamber to allow formation of dense DNA brushes. The spatial arrangement of the different brush configurations in the chamber was usually randomized and modified between experimental repeats.

Antibodies and ribosome deposition

Biotinylated anti–HA-biotin antibodies (50 μg/ml; High Affinity, 3F10 clone, Sigma-Aldrich) were mixed with SA at a molar ratio of 1:1.5 in 1× PBS and incubated for 30 min on ice, followed by dilution to 50 nM in 1× PBS. SA–anti-HA conjugates were applied to the chamber without prior rinsing of the DNA droplets to prevent smearing of SA-DNA on the surface. The chamber was washed several times with 1× PBS followed by rinsing with 50 mM potassium–Hepes buffer (pH 7), never drying the surface.

For experiments with surface-bound ribosomes, the chip was washed with RB after antibody deposition and incubation and then replaced by a 2 μM solution of purified ribosomes in RB, of which ~100 to 200 nM were estimated to be modified with L9-HA. After further 2-hour incubation at 4°C, the chamber was washed intensively with RB to remove nonspecifically adsorbed ribosomes.

On-chip cell-free gene expression reactions

The chip was positioned on a temperature-controlled holder set at 17°C placed on an upright microscope (Olympus BX51WI). Humidity in the room was reduced to avoid condensation on the prism. The potassium-HEPES buffer in the chamber was exchanged with PURExfrex2.0 (exchanging four times with fresh 40 μl of PURExfrex2.0 solution), supplemented with PEG 8000 and DFHBI-1T (Lucerna, NY) at final concentrations of 4% and 60 μM, respectively. PEG was found to enhance the reaction as can be seen in fig. S4A. For direct in situ labeling of r-proteins using unnatural fluorescent amino acids, the reaction was supplemented with CloverDirect ATTO655-X-AF amber (CosmoBio, Japan). On-chip expression reactions with some genes in the solution were supplemented with plasmids at a final concentration of 2 nM each, up to a total of 42 nM, depending on the number of different plasmids added. Expression reactions with immobilized ribosomes were supplemented with 1 μM purified SSU by sucrose gradient (a gift of A. Yonath). The chamber was sealed with a glass coverslip, and the temperature was then switched to 37°C to initiate gene expression.

Imaging

The microscope was positioned on a motorized stage (Scientifica). It was equipped with optical filter sets for excitation at 488 and 647 nm and a fluorescent light source (EXFO X-Cite 120Q) to allow epifluorescence microscopy. Two-color TIRF microscopy was performed by coupling two lasers (OBIS 488-150 LS and OBIS 647 LX, Coherent) into a single-mode optical fiber (OZ optics). The beam was then collimated and directed on the prism using a goniometer (Thorlabs) (fig. S1A). Epifluorescence and TIRF images were taken with Andor iXon Ultra camera (Andor Technology plc., Belfast, UK) and 10× Olympus objective. The stage, the microscope, the lasers, and the camera were controlled by LabVIEW (National Instruments).

Data analysis

Images were analyzed with ImageJ and Mathematica 11 (Wolfram Research). The fluorescent time traces were evaluated as described in fig. S1. When presented as color maps (Figs. 3 and 4, and figs. S7 to S10), fluorescent signals were normalized by the maximal signal obtained in each experiment. The time of initial signal detection t_0 was determined for each gene configuration as presented in fig. S1F. The maximal fluorescent signal f_{max} of each dynamic trace was normalized by the highest f_{max} that was obtained in each particular experiment. For example, in Figs. 1E and 2C, f_{max} of each r-protein–HA was normalized by the f_{max} of the S17-HA configuration. In Fig. 4B, each f_{max} was normalized by the f_{max} of the 2F/a1 configuration. For the Venn diagrams presented in Figs. 3 and 4, f_{max} was normalized similarly to the color maps according to the maximal signal in each experiment. All values represent averages of three different experiments.

SUPPLEMENTARY MATERIALS

Supplementary material for this article is available at http://advances.sciencemag.org/cgi/content/full/6/16/eaaz6020/DC1

View/request a protocol for this paper from *Bio-protocol*.

REFERENCES AND NOTES

1. W. A. Held, B. Ballou, S. Mizushima, M. Nomura, Assembly mapping of 30 S ribosomal proteins from Escherichia coli. Further studies. *J. Biol. Chem.* **249**, 3103–3111 (1974).
2. M. Herold, K. H. Nierhaus, Incorporation of six additional proteins to complete the assembly map of the 50 S subunit from Escherichia coli ribosomes. *J. Biol. Chem.* **262**, 8826–8833 (1987).

3. G. M. Culver, H. F. Noller, Efficient reconstitution of functional Escherichia coli 30S ribosomal subunits from a complete set of recombinant small subunit ribosomal proteins. *RNA* **5**, 832–843 (1999).
4. A. M. Mulder, C. Yoshioka, A. H. Beck, A. E. Bunner, R. A. Milligan, C. S. Potter, B. Carragher, J. R. Williamson, Visualizing ribosome biogenesis: Parallel assembly pathways for the 30S Subunit. *Science* **330**, 673–677 (2010).
5. H. Kim, S. C. Abeysirigunawarden, K. Chen, M. Mayerle, K. Ragunathan, Z. Luthey-Schulten, T. Ha, S. A. Woodson, Protein-guided RNA dynamics during early ribosome assembly. *Nature* **506**, 334–338 (2014).
6. P. L. Luisi, F. Ferri, P. Stano, Approaches to semi-synthetic minimal cells: A review. *Naturwissenschaften* **93**, 1–13 (2006).
7. A. C. Forster, G. M. Church, Towards synthesis of a minimal cell. *Mol. Syst. Biol.* **2**, 45 (2006).
8. V. Noireaux, Y. T. Maeda, A. Libchaber, Development of an artificial cell, from self-organization to computation and self-reproduction. *Proc. Natl. Acad. Sci. U.S.A.* **108**, 3473–3480 (2011).
9. M. C. Jewett, B. R. Fritz, L. E. Timmerman, G. M. Church, In vitro integration of ribosomal RNA synthesis, ribosome assembly, and translation. *Mol. Syst. Biol.* **9**, 678 (2013).
10. D. Tamaru, K. Amikura, Y. Shimizu, K. H. Nierhaus, T. Ueda, Reconstitution of 30S ribosomal subunits in vitro using ribosome biogenesis factors. *RNA* **24**, 1512–1519 (2018).
11. J. Li, W. Haas, K. Jackson, E. Kuru, M. C. Jewett, Z. H. Fan, S. Gygi, G. M. Church, Cogenerating synthetic parts toward a self-replicating system. *ACS Synth. Biol.* **6**, 1327–1336 (2017).
12. O. Duss, G. A. Stepanyuk, J. D. Puglisi, J. R. Williamson, Transient protein-RNA interactions guide nascent ribosomal RNA folding. *Cell* **179**, 1357–1369.e16 (2019).
13. M. L. Rodgers, S. A. Woodson, Transcription increases the cooperativity of ribonucleoprotein assembly. *Cell* **179**, 1370–1381.e12 (2019).
14. H. Matsubayashi, T. Ueda, Purified cell-free systems as standard parts for synthetic biology. *Curr. Opin. Chem. Biol.* **22**, 158–162 (2014).
15. Y. Heyman, A. Buxboim, S. G. Wolf, S. S. Daube, R. H. Bar-Ziv, Cell-free protein synthesis and assembly on a biochip. *Nat. Nanotechnol.* **7**, 374–378 (2012).
16. Y. Efrat, A. M. Tayar, S. S. Daube, M. Levy, R. H. Bar-Ziv, Electric-field manipulation of a compartmentalized cell-free gene expression reaction. *ACS Synth. Biol.* **7**, 1829–1833 (2018).
17. S. A. Woodson, RNA folding and ribosome assembly. *Curr. Opin. Chem. Biol.* **12**, 667–673 (2008).
18. M. W. T. Talkington, G. Siuzdak, J. R. Williamson, An assembly landscape for the 30S ribosomal subunit. *Nature* **438**, 628–632 (2005).
19. M. Wieland, B. Berschneider, M. D. Erlacher, J. S. Hartig, Aptazyme-mediated regulation of 16S ribosomal RNA. *Chem. Biol.* **17**, 236–242 (2010).
20. G. S. Filonov, C. W. Kam, W. Song, S. R. Jaffrey, In-gel imaging of RNA processing using broccoli reveals optimal aptamer expression strategies. *Chem. Biol.* **22**, 649–660 (2015).
21. S. C. Walker, J. M. Avis, G. L. Conn, General plasmids for producing RNA in vitro transcripts with homogeneous ends. *Nucleic Acids Res.* **31**, e82 (2003).
22. Y. Shimizu, A. Inoue, Y. Tomari, T. Suzuki, T. Yokogawa, K. Nishikawa, T. Ueda, Cell-free translation reconstituted with purified components. *Nat. Biotechnol.* **19**, 751–755 (2001).
23. J. Garamella, R. Marshall, M. Rustad, V. Noireaux, The All E. coli TX-TL toolbox 2.0: A platform for cell-free synthetic biology. *ACS Synth. Biol.* **5**, 344–355 (2016).
24. T. M. Earnest, J. Lai, K. Chen, M. J. Hallock, J. R. Williamson, Z. Luthey-Schulten, Toward a whole-cell model of ribosome biogenesis: Kinetic modeling of SSU assembly. *Biophys. J.* **109**, 1117–1135 (2015).
25. C. J. Weitzmann, P. R. Cunningham, K. Nurse, J. Ofengand, Chemical evidence for domain assembly of the Escherichia coli 30S ribosome. *FASEB J.* **7**, 177–180 (1993).
26. S. C. Agalarov, G. Sridhar Prasad, P. M. Funke, C. D. Stout, J. R. Williamson, Structure of the S15,S6,S18-rRNA complex: Assembly of the 30S ribosome central domain. *Science* **288**, 107–113 (2000).
27. R. R. Samaha, B. O. Brien, T. W. O. Brient, H. F. Noller, Independent in vitro assembly of a ribonucleoprotein particle containing the 3′ domain of 16S rRNA. *Proc. Natl. Acad. Sci. U.S.A.* **91**, 7884–7888 (1994).
28. M. I. Recht, J. R. Williamson, Central domain assembly: Thermodynamics and kinetics of S6 and S18 binding to an S15-RNA complex. *J. Mol. Biol.* **313**, 35–48 (2001).
29. R. J. Gregory, M. L. Zeller, D. L. Thurlow, R. L. Gourse, M. J. Stark, A. E. Dahlberg, R. A. Zimmermann, Interaction of ribosomal proteins S6, S8, S15 and S18 with the central domain of 16 S ribosomal RNA from Escherichia coli. *J. Mol. Biol.* **178**, 287–302 (1984).
30. S. C. Abeysirigunawardena, H. Kim, J. Lai, K. Ragunathan, M. C. Rappé, Z. Luthey-Schulten, T. Ha, S. A. Woodson, Evolution of protein-coupled RNA dynamics during hierarchical assembly of ribosomal complexes. *Nat. Commun.* **8**, 492 (2017).
31. W. K. Ridgeway, D. P. Millar, J. R. Williamson, Quantitation of ten 30S ribosomal assembly intermediates using fluorescence triple correlation spectroscopy. *Proc. Natl. Acad. Sci. U.S.A.* **109**, 13614–13619 (2012).
32. S. Goto, S. Kato, T. Kimura, A. Muto, H. Himeno, RsgA releases RbfA from 30S ribosome during a late stage of ribosome biosynthesis. *EMBO J.* **30**, 104–114 (2011).
33. C. C. de Narvaez, H. W. Schaup, In vivo transcriptionally coupled assembly of *Escherichia coli* ribosomal subunits. *J. Mol. Biol.* **134**, 1–22 (1979).
34. A. Trauner, M. H. Bennett, H. D. Williams, Isolation of bacterial ribosomes with monolith chromatography. *PLOS ONE* **6**, e16273 (2011).
35. S. Uemura, R. Iizuka, T. Ueno, Y. Shimizu, H. Taguchi, T. Ueda, J. D. Puglisi, T. Funatsu, Single-molecule imaging of full protein synthesis by immobilized ribosomes. *Nucleic Acids Res.* **36**, e70 (2008).
36. Q. Liu, K. Fredrick, Intersubunit bridges of the bacterial ribosome. *J. Mol. Biol.* **428**, 2146–2164 (2016).
37. M. Tal, A. Silberstein, K. Møyner, In vivo reassembly of 30-S ribosomal subunits following their specific destruction by thermal shock. *Biochim. Biophys. Acta.* **479**, 479–496 (1977).
38. D. Bracha, E. Karzbrun, S. S. Daube, R. H. Bar-Ziv, Emergent properties of dense DNA phases toward artificial biosystems on a surface. *Acc. Chem. Res.* **47**, 1921–1921 (2014).

Acknowledgments: We thank Y. Barak for help with ribosome purification, N. Stern for reading the manuscript, and Y. Shimizu, T. Tlusty, and A. Libchaber for discussions. **Funding:** We acknowledge funding from the Israel Science Foundation (grant no. 1870/15), the Minerva Foundation (grant no. 712274), and the Human Frontier Science Program (grant no. RGP0043/2017). **Author contributions:** R.H.B.-Z. and S.S.D. conceived and supervised the project. S.S.D. performed the molecular cloning and biochemical experiments. M.L. designed and performed the experiments on chip. R.F. developed and realized the active surface-bound ribosomes. M.L. analyzed the data. All authors discussed the results and wrote the manuscript. **Competing interests:** R.H.B.-Z., S.S.D., M.L., and R.F. are inventors on a pending Israeli patent application related to this work filed by Yeda Research and Development Co. Ltd. (no. 269674, filed 25 September 2019). The authors declare that they have no other competing interests. **Data and materials availability:** All data needed to evaluate the conclusions in the paper are present in the paper and/or the Supplementary Materials. Additional data related to this paper may be requested from the authors.

Submitted 23 September 2019
Accepted 22 January 2020
Published 15 April 2020
10.1126/sciadv.aaz6020

Citation: M. Levy, R. Falkovich, S. S. Daube, R. H. Bar-Ziv, Autonomous synthesis and assembly of a ribosomal subunit on a chip. *Sci. Adv.* **6**, eaaz6020 (2020).

Science Advances

Autonomous synthesis and assembly of a ribosomal subunit on a chip

Michael Levy, Reuven Falkovich, Shirley S. Daube and Roy H. Bar-Ziv

Sci Adv **6** (16), eaaz6020.
DOI: 10.1126/sciadv.aaz6020

Science Advances (ISSN 2375-2548) is published by the American Association for the Advancement of Science, 1200 New York Avenue NW, Washington, DC 20005. The title *Science Advances* is a registered trademark of AAAS.